REVISTA MATÉRIA V.30
ISSN 1517-7076 articles e20250614, 2025

Effects of cold rolling on the microstructure and crystallographic texture of aluminum alloy 7108

Saul Hissaci de Souza[1], Leandro Gomes de Carvalho[1], Nelson Batista de Lima[2], Rene Ramos de Oliveira[2], Angelo Fernando Padilha[1]

[1]Universidade de São Paulo, Escola Politécnica, Departamento de Engenharia Metalúrgica e de Materiais. Av. Prof. Mello de Moraes, 2463, 05508-030, São Paulo, SP, Brasil.

[2]Instituto de Pesquisas Energéticas e Nucleares. Av. Prof. Lineu Prestes, 2242, 05508-000, São Paulo, SP, Brasil.

e-mail: leandro.carvalho@usp.br, saulhso@usp.br, nblima@ipen.br, rolivier@ipen.br, padilha@usp.br

ABSTRACT

Herein, industrial-scale extruded profiles of aluminum alloy (AA) 7108 with rectangular cross-sections of dimensions 25.60 mm × 15.95 mm were used to investigate the effect of number of passes and strain rate on their crystallographic texture. After the initial microstructural and textural characterization, the samples were solution-annealed and cold-rolled using different numbers of passes to achieve the same degree of reduction. The samples that were cold-rolled for a few number of passes exhibited a remaining Cube texture component {001} <001> (similar to that observed in the AA 7108 as-received bars), a Goss component {011} <001>, and a Brass component {011} <211>. In contrast, the samples rolled for a high number of passes demonstrated only a strong Goss component {011} <001>.

Keywords: Aluminum alloys; AA 7108; Crystallographic texture; Cold rolling; Microstructure.

1. INTRODUCTION

Aluminum alloy (AA) 7108 is a precipitation-hardenable AA of the ternary Al–Zn–Mg system [1, 2]. After aging, this alloy exhibits intermediate mechanical strength (yield strength of approximately 350 MPa), which is lower than that of high-strength AAs, such as 7075 and 2024 [1, 3], and higher than that of most 6XXX alloys [1, 4]. AA 7108 can be applied to land transportation vehicles without any concerns related to stress corrosion cracking, which is a common issue associated with other 7XXX and 2XXX high-strength AAs [1–3]. Only a few studies are available on the alloy AA 7108, particularly on its crystallographic texture [5]. Strain-hardening, although rarely studied in this alloy, can be used as an alternative for increasing its mechanical strength. However, it varies with position along the thickness of the sample as a function of the crystallographic texture of the sample [6].

The crystallographic texture of metallic alloys, and specifically aluminum alloys, is influenced by three primary factors: chemical composition, manufacturing process, and the resulting microstructure [7, 8]. While research has historically correlated the crystallographic texture of thin aluminum alloy sheets with earing during deep drawing [9], the scope of this work is limited to thick bars and does not address that particular issue.

During mechanical forming processes, such as extrusion or rolling, a metallic piece of metal is deformed to another shape and size, resulting in the generation of typical texture components [6]. Some rolling and recrystallization texture components of face-centered cubic (FCC) metals and alloys are listed in Table 1 [10, 11].

Besides the mechanical process, different processing parameters result in a variety of textures. JAYAGANTHAN *et al.* [12] reported that increasing the amount of deformation of AA 7075 plates under cryogenic rolling resulted in the progressive weakening of the texture components. WANG *et al.* [13] demonstrated the possibility of obtaining different rolling textures using different heating rates during the solution-treatment of an Al–Mg–Si–Cu alloy. Herein, an extruded bar of the AA 7108 was solution-annealed and cold-rolled for different numbers of passes to achieve the same degree of reduction in the thickness. Two different forming processes namely, hot extrusion and cold rolling, were chosen to perform texture experiments. The microstructures and crystallographic textures of the samples were investigated after each step. This work aims to evaluate the influence of the number of passes during the rolling process on the crystallographic texture of AA 7108.

Corresponding Author: Leandro Gomes de Carvalho Received on 12/07/2025 Accepted on 30/09/2025

DOI: https://doi.org/10.1590/1517-7076-RMAT-2025-0614

Table 1: Typical texture components for FCC metals [10, 11].

NOTATION	MILLER INDICES {HKL} <UVW>	POSSIBLE EULER ANGLES Φ_1, Φ, Φ_2	TEXTURE
C, Copper	{112} <111>	90°, 35°, 45°	Rolling
S	{123} <634>	59°, 37°, 63°	Rolling
B, Brass	{011} <211>	35°, 45°, 0°	Rolling
G, Goss	{011} <100>	0°, 45°, 0°	Rolling
Cube	{001} <100>	0°, 0°, 0°	Recrystallization
Rotated Cube	{001} <110>	45°, 0°, 0°	Recrystallization

2. MATERIALS AND METHODS

The AA 7108 bar with a rectangular cross-section (25.60 mm × 15.95 mm) was obtained from the *Companhia Brasileira de Alumínio (CBA)*. The bar was extruded from a billet of 203.2 mm diameter at a temperature of 450 °C using a horizontal press of 2800 tons. The composition of the alloy, provided by supplier, is listed in Table 2.

Table 2: Chemical composition of the AA 7108 used in this study (% mass).

Ti	Si	Cr	Fe	Mg	Zr	Zn	Al
0.05	0.05	0.01	0.10	1.03	0.20	4.96	Balance

Samples from the bar were cut, ground, and polished using 6, 3, and 1 μm diamond pastes. Subsequently, colloidal silica polishing was performed. The polished specimens were subjected to anodic oxidation in tetrafluoroboric acid (1.8%) at 20 V using AA 1050 as the cathode. The samples were analyzed using an optical microscope under polarized light. Specimens were prepared for microtexture analysis based on electron backscatter diffraction (EBSD) using an FEI–Inspect 50 scanning electron microscope (SEM) and macrotexture analysis based on X-ray diffraction (XRD) using the Rigaku DMAX 2000 (MoKα radiation). Furthermore, the orientation distribution functions (ODFs), and grain-orientation maps were obtained for the surface and layers below the surface of the extrusion bars to investigate the textures (Figure 1).

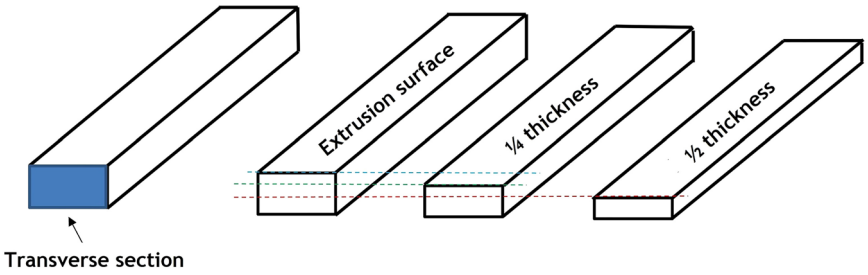

Figure 1: Scheme of the analyzed surfaces of AA 7108 extruded bar.

The total error in X-ray diffraction (XRD) measurements of crystallographic texture can be attributed to several sources, including systematic, statistical, mathematical, and numerical errors. Systematic errors often result from inadequate sample preparation [7]. The statistical significance of these measurements is directly tied to the number of grains analyzed, with XRD providing a representative sample due to its large irradiated area and notable beam penetration depth [7, 14]. Mathematical errors stem from the finite terms of expansion series (truncation) and the integration of discrete functions used to generate pole figures. Lastly, numerical errors arise from the required rounding of significant figures during each calculation [7]. Careful measurement practices and recent technological advances have significantly reduced the various types of errors previously mentioned. For example, the close agreement between pole figures obtained from X-ray diffraction (XRD) and automated electron backscatter diffraction (EBSD) is a strong indication that errors are being minimized across different texture measurement methods [15].

An extruded profile was cut into several pieces, solution-annealed at 490 °C (5 h), and quenched in water. Subsequently, the samples were cold-rolled for different number of passes to achieve certain degrees of

reduction in thickness (Table 3). Finally, the cold-rolled samples were analyzed using polarized light optical microscope and XRD to determine the macrotexture.

Table 3: Samples used in this study**.**

SAMPLE NAME	DEGREE OF REDUCTION (THICKNESS)	NUMBER OF PASSES
A30	33.7%	6
B30	33.7%	12
A60	63.6%	11
B60	63.6%	22

Vickers hardness measurements were performed on the extrusion surface of AA7108 alloy samples. The samples were tested in four conditions: 'as received', raw cast, solution-annealed, and mechanic-thermally treated. A Shimadzu hardness tester with a 100 g load was used, with 15 measurements taken on each sample.

3. RESULTS AND DISCUSSION

Figure 2 demonstrates the microstructure of the extrusion surface of AA 7108. Only fully recrystallized grains with approximately equiaxial shapes are observed, indicating that dynamic (or metadynamic) recrystallization occurs after (or during) the hot extrusion process. In addition, the well-defined colors of grains indicate a microstructure with a low density of dislocations or dislocation arrangements that are eliminated after migration of grain boundaries during recrystallization [16]. Thus, high strain rates and deformation temperatures (parameters used in the hot extrusion process) favor the occurrence of dynamic recrystallization in FCC metals and alloys [17].

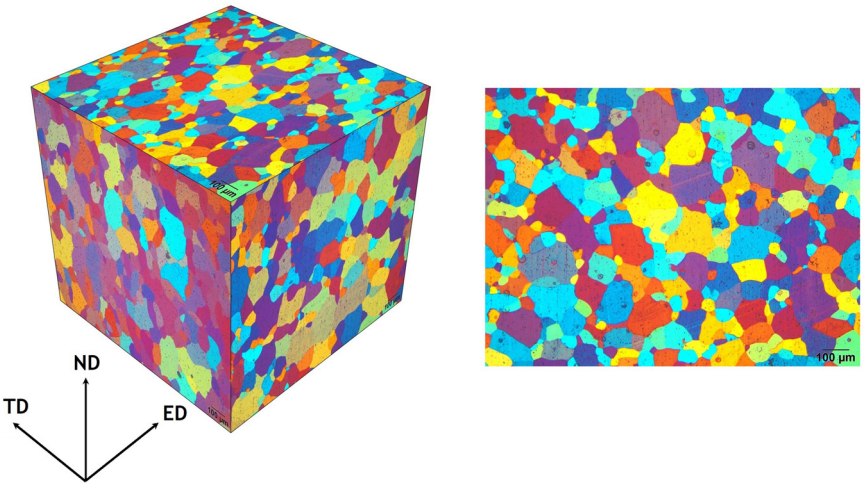

Figure 2: Optical micrographs (obtained under polarized light) of AA 7108 samples. The images indicate a fully recrystallized grain structure. ND, TD and ED indicate normal, transverse, and longitudinal extrusion direction, respectively.

Figure 3 exhibits the microstructure of the transverse section of AA 7108. A layer of coarse grains with an approximate thickness of 300 µm is observed near the extrusion surface. Different colors of the grains at the periphery and those located at the center of the transverse section indicate their different crystallographic orientations. A detailed study focused on the coarse grain layer and its crystallographic texture was conducted by SOUZA *et al.* [18].

Figure 4 shows the EBSD orientation maps of the surface and center of the extrusion bar (referred to as ½ thickness) and ODFs for $\varphi_2 = 0°$. These orientation maps depict a substantial difference in the grain size at different locations of the extrusion surface. In addition, the Goss texture component (Euler angles: $\varphi_1 = 0°$, $\phi = 45°$, $\varphi_2 = 0°$) at the center of the sample is not observed near the periphery. In contrast, a strong Cube component ($\varphi_1 = 0°$, $\phi = 0°$, $\varphi_2 = 0°$) is observed for both regions, suggesting that the appearance of a Goss component is favored at low strain rates. A similar result was reported by MARTINS and PADILHA [19] when an AA 3003 plate was processed using a twin-roll caster process.

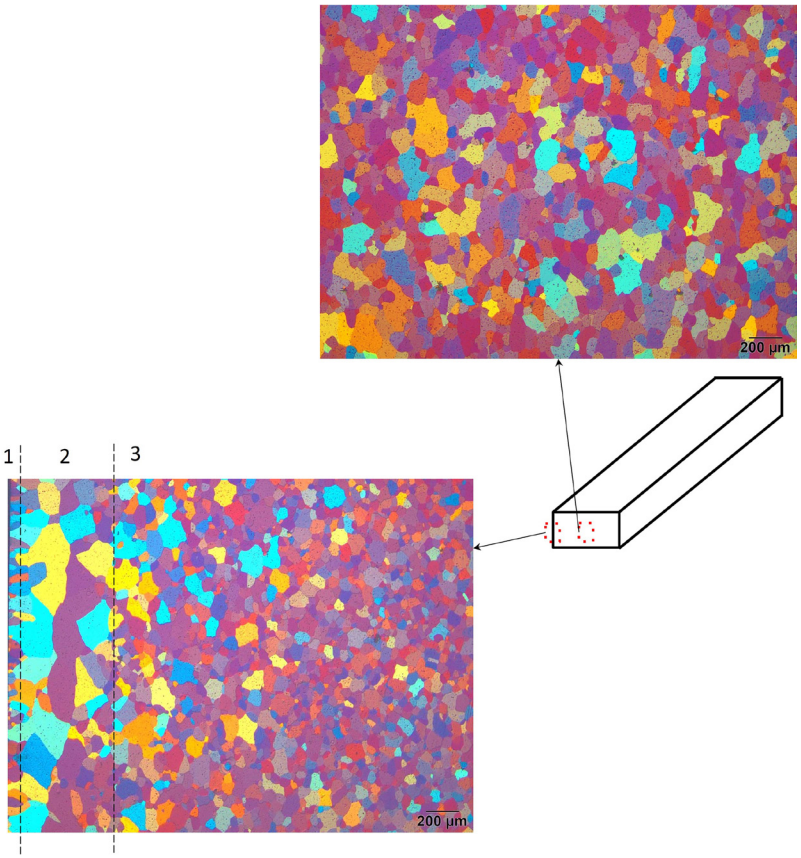

Figure 3: Optical micrographs, obtained under polarized light, of the transverse section of AA 7108. The images indicate the size difference between the grains present at the center and those at the periphery of the extruded bars.

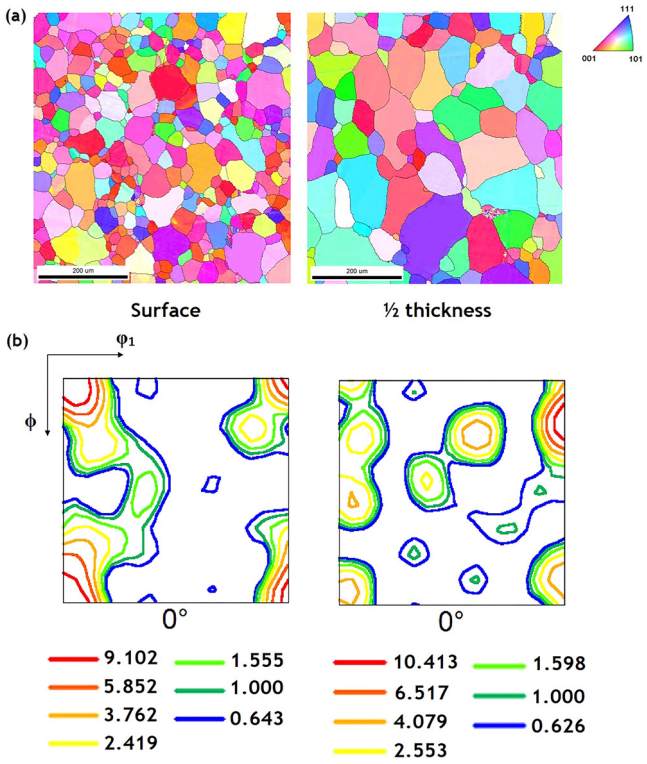

Figure 4: Texture analyses of AA 7108 extruded bars: (a) Electron backscatter diffraction (EBSD) orientation maps for the surface and center of the extruded bars; (b) the orientation distribution function (ODF) for $\varphi_2 = 0°$.

ODFs (φ_2 = 0°) obtained from XRD (macrotexture) analyses are demonstrated in Figure 5. A Cube component is observed on the surface region, whereas both the Cube and Goss components are observed in the ½ thickness. In ¼ thickness, the transition crystallographic components are identified between the surface and center. These results further confirm that the appearance of the Goss component is related to low strain rates.

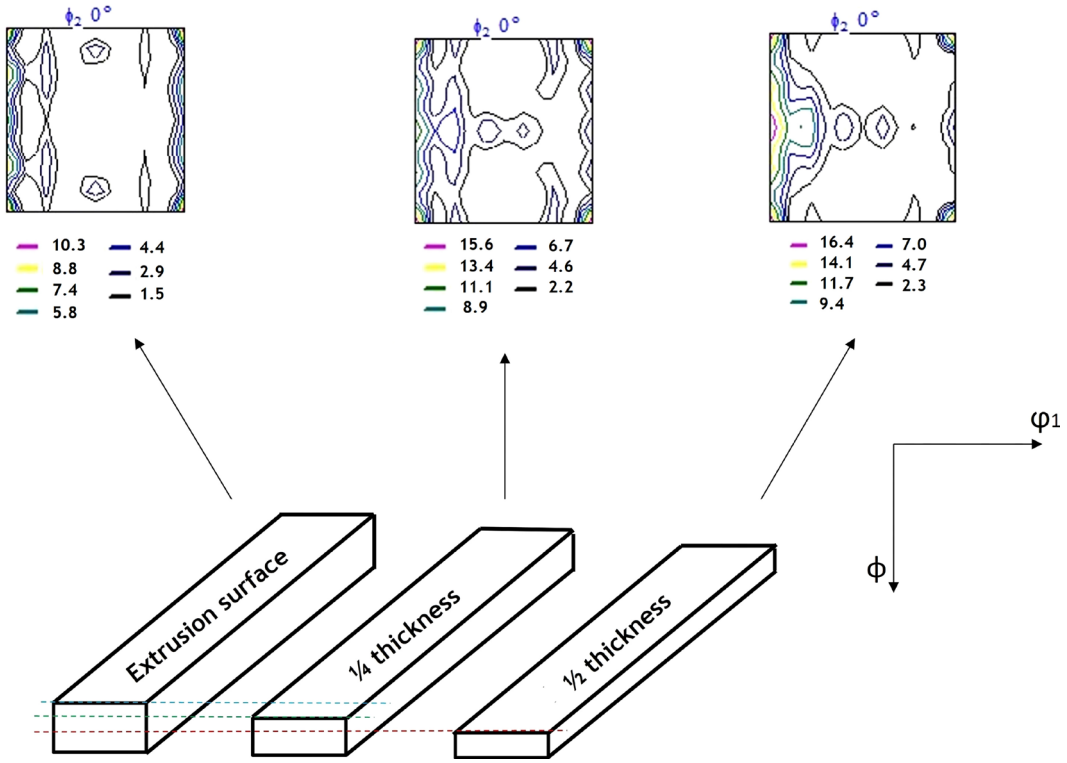

Figure 5: Orientation distribution function (φ_2 = 0°) obtained by X-ray diffraction analyses of the surface and ¼ and ½ thickness region of the AA 7108 extruded bar.

Figure 6 depicts the fiber plots of the extruded bar along the <001> direction. The intensity of the Goss component increases with decreasing thickness toward the center of the sample. This component is not typically observed in AAs after recrystallization [11, 20] or secondary recrystallization [21]. However, the Goss texture was reported in wrought AAs [11], which could be attributed to lower cooling rates at the center of the bar than those at the periphery during mechanothermal processing [13].

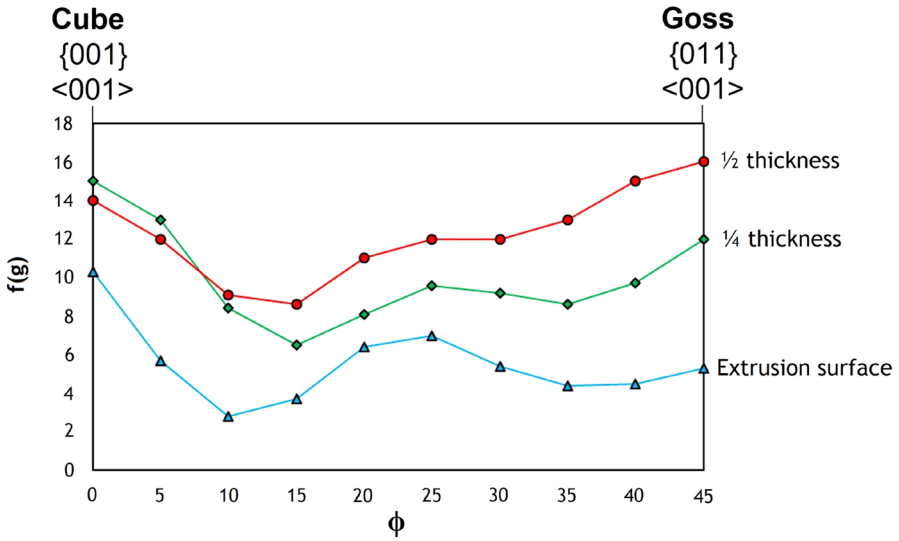

Figure 6: Fiber plots along <100> direction (φ_1 = 0°, φ_2 = 0°, and 0 < ϕ < 45°) of AA 7108 extruded bar.

The micrographs of the rolling surfaces of the cold-rolled samples were obtained using a polarized light optical microscope (Figure 7). Each micrograph is represented with the sample name and corresponding degree of reduction in thickness (A30, B30, A60, and B60). In addition, the rolling directions are indicated at the top of each micrograph. Samples 'B' were processed through higher number of passes than samples 'A', resulting into larger size of the grains of samples 'B' than that of samples 'A'. Additionally, samples 'B' exhibit a well-defined color of the grains, indicating that 1) the difference in orientation between adjacent subgrains is small, and 2) the dislocation density of samples 'B' is lower than that of samples 'A'. These results can be attributed to the effect of strain rate. Samples 'B' were deformed at a lower strain than that of samples 'A'; therefore, more time is available for dislocation movement and rearrangement in samples 'B', resulting in the observed color in optical micrographs.

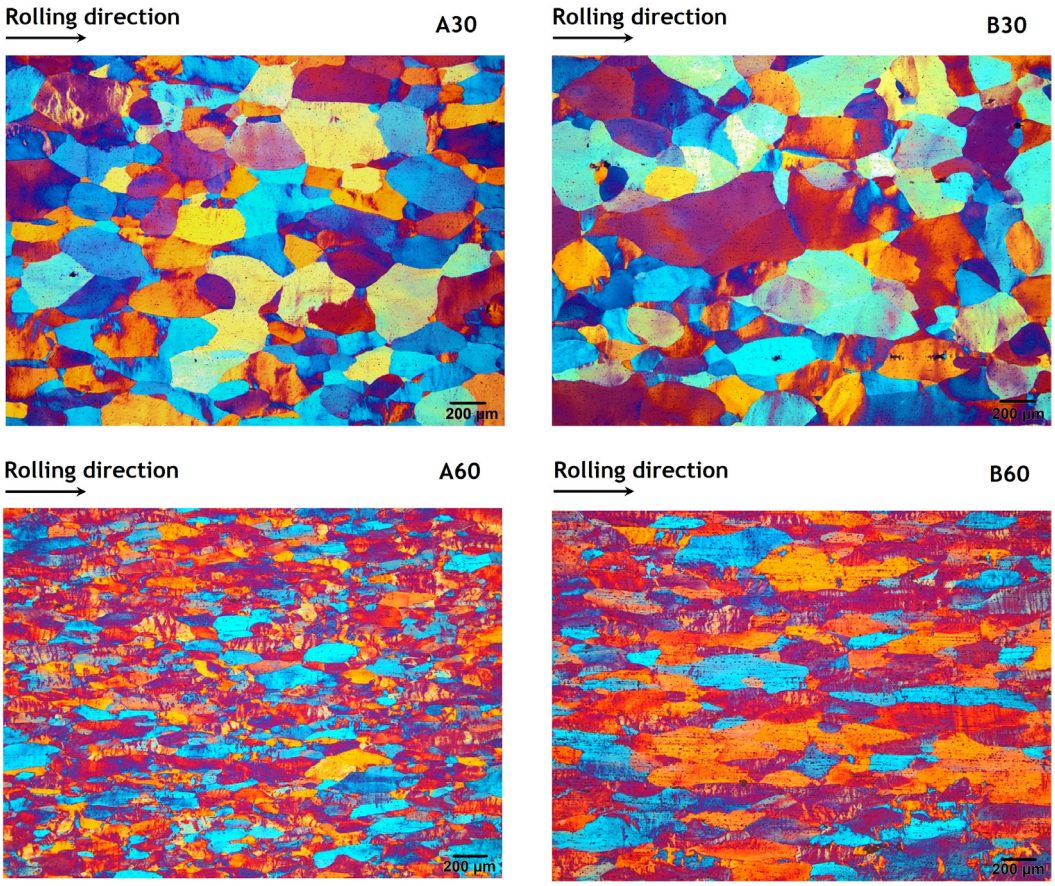

Figure 7: Optical micrographs, obtained under polarized light, of AA 7108 cold-rolled samples. The rolling direction and the degree of reduction in thickness are indicated on the top of each image.

Figure 8 exhibits ODFs ($\varphi_2 = 0°$) obtained by performing XRD analyses of the rolled samples. The samples 'A' demonstrate a remaining Cube component texture and a strong Goss component. In contrast, samples 'B' exhibit only a strong Goss texture. Fiber plots were analyzed further to understand these differences in the texture of samples 'A' and 'B'.

Figure 9 depicts the relative intensities of a few texture components along the <001> direction for samples 'A' and 'B'. A substantial difference is observed between the texture components of 'A30' and 'B30'; the sample 'B30' exhibits a strong Goss component, whereas a remaining Cube texture (from the

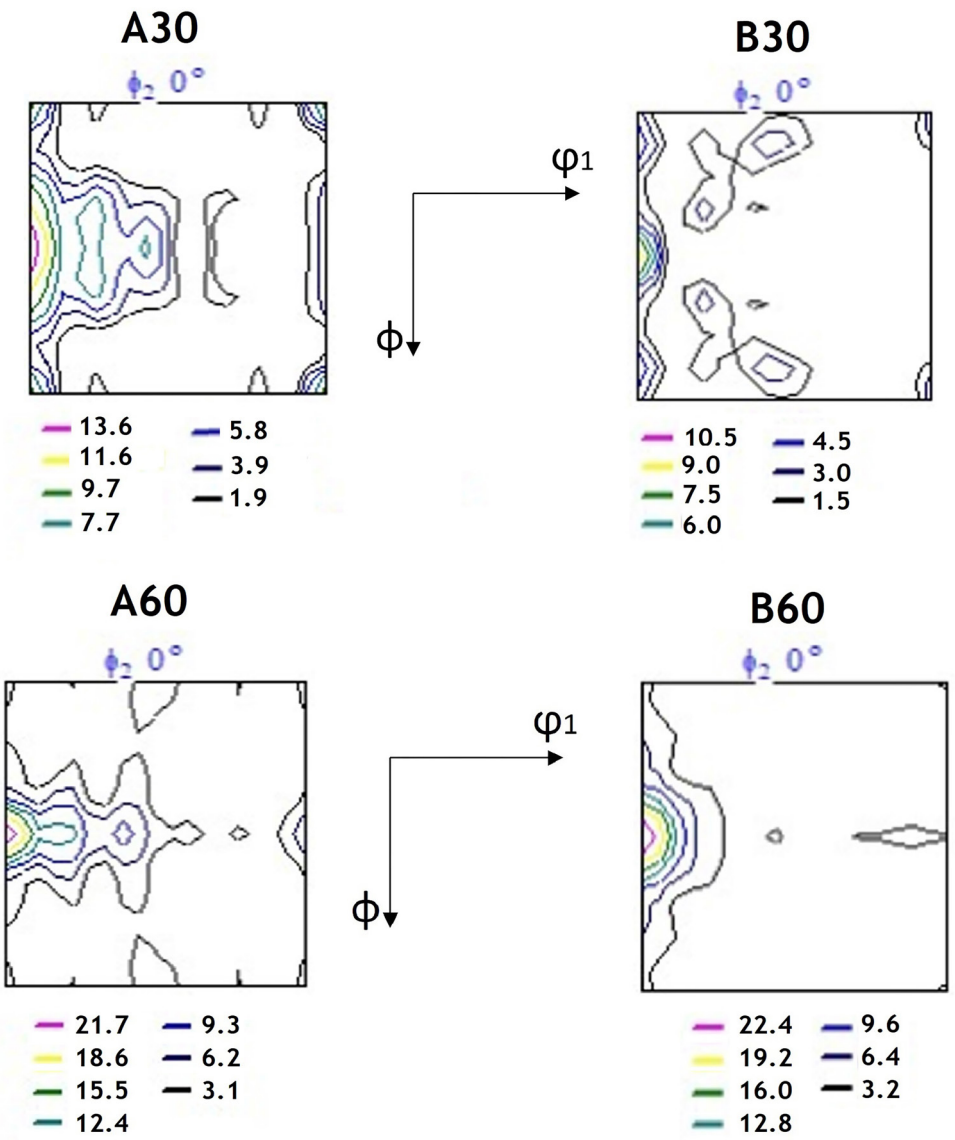

Figure 8: Orientation distribution function ($\varphi_2 = 0°$) obtained by X-ray diffraction analyses of AA 7108 cold-rolled samples.

extruded bar) in addition to a strong Goss texture is observed in sample 'A30'. This indicates that a low strain rate is efficient in removing the previous Cube texture and promoting the appearance of a Goss texture. In contrast, no significant differences are observed between samples 'A60' and 'B60' in the <001> direction.

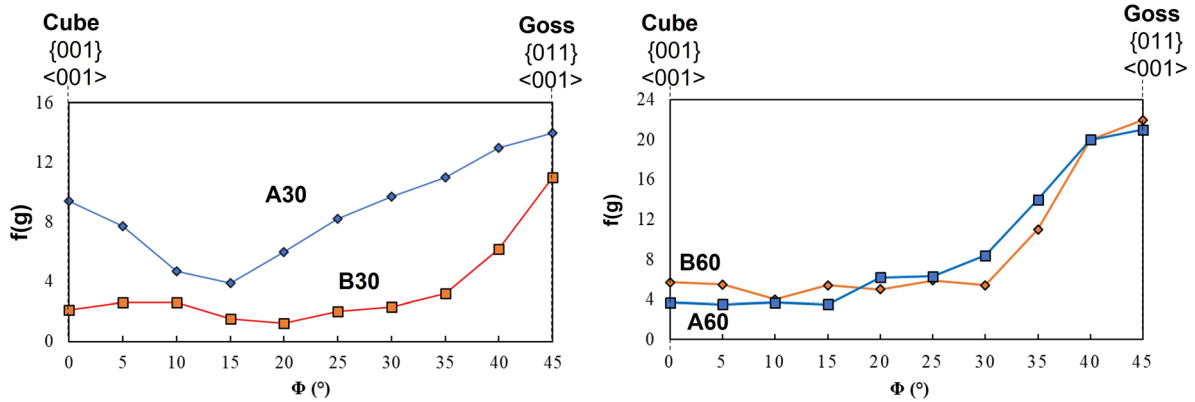

Figure 9: Fiber plots along <100> direction ($\varphi_1 = 0°$, $\varphi_2 = 0°$, and $0 < \phi < 45°$) of AA 7108 cold-rolled samples.

Figure 10 demonstrates the α-fibers ($\varphi_2 = 0°$, $\phi = 45°$, and $0 < \varphi_1 < 45°$) for samples 'A' and 'B'. The strain rate does not exhibit a notable influence on the rolling process. Brass ($\varphi_1 = 35°$, $\phi = 45°$ and $\varphi_2 = 0°$) texture component is observed in the samples, which are rolled for a smaller number of passes at a high strain rate. Literature suggests that a certain degree of anisotropy is a desirable feature for the deep-drawing process because it leads to a reduction in earing defects [22, 23]. Therefore, a combination of texture components, such as Cube (a typical FCC recrystallization texture) and Goss and Brass and/or S (typical rolling textures for FCC metals and alloys), are required for such applications to avoid drawing defects [23, 24]. Thus, samples rolled using a limited number of passes (samples 'A') are more effective at addressing the challenges posed by specific texture components during this mechanical process.

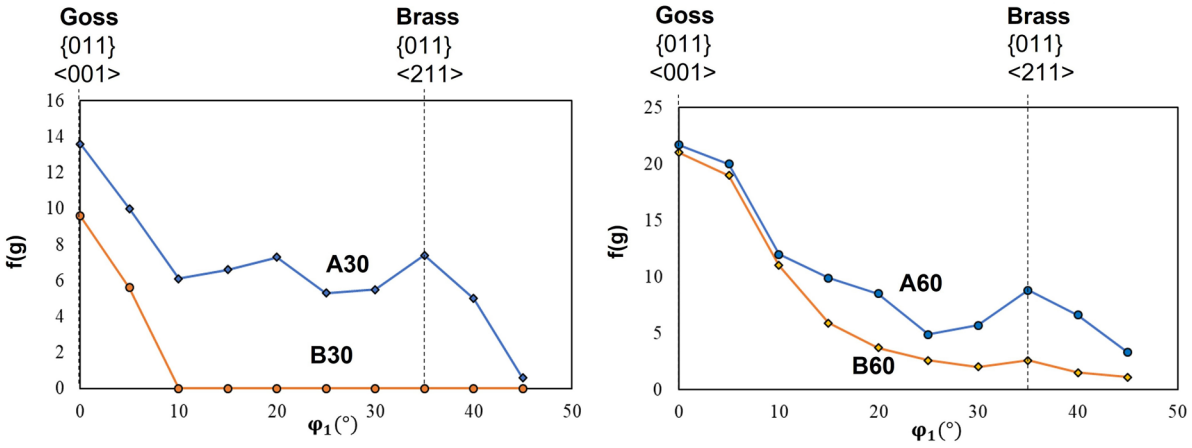

Figure 10: α-fiber plots ($0 < \varphi_1 < 45°$, $\phi = 45°$, and $\varphi_2 = 0°$) of AA 7108 cold-rolled samples.

Most published results on crystallographic texture focus on rolled materials. The rolling textures of face-centered cubic (FCC) metals and alloys are strongly dependent on their respective stacking fault energies (SFE). Pure aluminum has a high SFE of approximately 170 mJ/m^2, and the alloying elements in AA 7108 (primarily Zn and Mg) are not sufficient to modify it significantly [25, 26].

After solution annealing, it was estimated that over 90% of the alloy's solute concentration was in a solid solution. However, using SEM/EDS, a few dispersed micrometric particles of the types $Al_3(Ti,Zr)$ and $(Al)_X(Fe,Mg,Zn)_Y$ were detected in the matrix [5]. The presence of these particles generally contributes to a weakening of the deformation texture. They do this by concentrating plastic deformation (specifically, dislocations) around themselves, which inhibits the formation of deformation bands (e.g., kink, transition, and shear bands) [16, 19]. This weakening effect is further accentuated by the subsequent particle-stimulated nucleation (PSN) of recrystallization [27].

Table 4 presents the results of Vickers microhardness performed on AA7108 samples under various conditions. A notable finding is the decrease in microhardness for the sample that was solution-annealed at 490 °C for 5 hours. This behavior is caused by the dissolution of $MgZn_2$ precipitates (or Guinier-Preston zones), which are the main precipitation hardening phases in the alloy [28].

Table 4 shows that the number of passes has a greater effect on hardness at lower reduction degrees. The higher hardness of sample B30 compared to sample A30 is likely due to their distinct texture behaviors, as seen in Figures 9 and 10. The {011}-oriented grains, specifically Brass and Goss textures, demonstrate a greater tendency to develop higher dislocation densities than grains with {001} orientations, such as the Cube texture. This difference is attributed to the crystallographic slip systems and their response to deformation [29]. Furthermore, sample B was deformed more slowly than sample A. This slower deformation rate allowed more time for dislocation movement and rearrangement, likely into a cellular structure, which led to a decrease in hardness values. However, the hardness difference between samples A and B is less pronounced at the higher deformation degree (63.6%). This could be due to a significantly elevated dislocation density, which makes the formation of new dislocation cells less feasible, resulting in minimal differences between the samples [30].

Table 4: Vickers microhardness for AA7108 **s**amples that were cold rolled in different ways**.**

SAMPLE NAME	DEGREE OF REDUCTION (THICKNESS)	NUMBER OF PASSES	HV 0.1
'As received'	–	–-	84.3 ± 5.8
Solution-annealed at 490 °C for 5 h	–		53.8 ± 1.6
A30	33.7%	6	90.8 ± 3.1
B30	33.7%	12	84.2 ± 3.5
A60	63.6%	11	107.5 ± 2.3
B60	63.6%	22	105.3 ± 2.8

4. CONCLUSIONS

A hot-extruded rectangular cross-sectional bar AA 7108 exhibited a fully recrystallized and nearly equiaxial grain structure. A peripheral grain growth zone (PCGZ) was observed at the edges of the transverse section. In addition, the alloy exhibited a strong Cube texture on the extrusion surface and strong Goss component in the half-thickness region. These are the two common texture components of AA, which are attributed to the recrystallization and cold rolling, respectively. After cold rolling, the samples that deformed owing to a higher number of passes (or a lower strain rate), demonstrated a few deformed grains and strong Goss texture, whereas samples strained because of a lower number of passes demonstrated a highly deformed grain structure and a remaining Cube texture apart from the Goss component. This information can be useful in optimizing the microstructure and properties of the alloy.

5. ACKNOWLEDGMENTS

One of the authors (Saul Hissaci de Souza) would like to thank the Coordenação de Aperfeiçoamento de Pessoal de Nível Superior, Brazil (CAPES-Brazil), for granting a doctoral scholarship (Finance Code 001). We also would like to thank Editage for English language reviewing.

6. BIBLIOGRAPHY

[1] KAUFMAN, J.G., *Introduction to aluminum alloys and tempers*, 1 ed., Materials Park, ASM International, 2019.

[2] HATTORI, C.S., ALMEIDA, G.F.C., GONÇALVES, R.L.P., *et al*., "Microstructure and fatigue properties of extruded aluminum alloys 7046 and 7108 for automotive applications", *Journal of Materials Research and Technology*, v. 14, pp. 2970–2981, 2021. doi: http://doi.org/10.1016/j.jmrt.2021.08.085.

[3] OÑORO, J., MORENO, A., RANNINGER, C., "Stress corrosion cracking model in 7075 aluminium alloy", *Journal of Materials Science*, v. 24, n. 11, pp. 3888–3891, 1989. doi: http://doi.org/10.1007/BF01168951.

[4] JINAN, W.T., PADILHA, A.F., "Microstructure evolution during the extrusion of a 6351 aluminum alloy tube", *REM - International Engineering Journal*, v. 72, n. 3, pp. 479–484, 2019. doi: http://doi.org/10.1590/0370-44672018720174.

[5] SOUZA, S.H., " *Study of the work hardening, recrystallization and evolution of the crystallographic texture of aluminum alloy AA 7108*", Tese de D.Sc., Universidade de São Paulo, São Paulo, 2021.

[6] PÉROCHEAU, F., DRIVER, J.H., "Texture gradient simulations for extrusion and reversible rolling of FCC metals", *International Journal of Plasticity*, v. 16, n. 1, pp. 73–89, 2000. doi: http://doi.org/10.1016/S0749-6419(99)00048-0.

[7] BUNGE, H.J., *Texture analysis in materials science: mathematical methods*, 2 ed., Amsterdam, Elsevier, 2013.

[8] BARONY, N.B., JORGE, I.C.S., SILVA, A.S., *et al*., "Comportamento mecânico e textura de chapas finas das ligas de alumínio 5052 e 5050C", *Matéria*, v. 29, n. 2, e20230321, 2024. doi: http://doi.org/10.1590/1517-7076-rmat-2023-0321.

[9] STÜWE, H.P., FAUSTMAN, J., *Introduccion a las texturas de los materiales metálicos*, Madrid, Editorial Montorvo, 1969.

[10] ZHANG, L., WANG, Y., YANG, X., *et al*., "Texture, microstructure and mechanical properties of 6111 aluminum alloy subject to rolling deformation", *Materials Research*, v. 20, n. 5, pp. 1360–1368, 2017. doi: http://doi.org/10.1590/1980-5373-mr-2017-0549.

[11] HIRSCH, J., "Texture evolution during rolling of aluminum alloys", In: *Light Metals – Warrendale Proceedings*, pp. 1071–1077, New Orleans, Mar. 2008.

[12] JAYAGANTHAN, R., BROKMEIER, H.G., SCHWEBKE, B., *et al*., "Microstructure and texture evolution in cryorolled Al 7075 alloy", *Journal of Alloys and Compounds*, v. 496, n. 1–2, pp. 183–188, 2010. doi: http://doi.org/10.1016/j.jallcom.2010.02.111.

[13] WANG, X., GUO, M., CAO, L., *et al*., "Effect of heating rate on mechanical property, microstructure and texture evolution of Al–Mg–Si–Cu alloy during solution treatment", *Materials Science and Engineering A*, v. 621, pp. 8–17, 2015. doi: http://doi.org/10.1016/j.msea.2014.10.045.

[14] RANDLE, V., ENGLER, O., *Introduction to texture analysis: macrotexture, microtexture and orientation mapping*, Amsterdam, Gordon and Breach Science Publishers, 2002.

[15] WRIGHT, S.I., NOWELL, M.M., BINGERT, J.F., "A comparison of textures measured using X-ray and electron backscatter diffraction", *Metallurgical and Materials Transactions. A, Physical Metallurgy and Materials Science*, v. 38, n. 8, pp. 1845–1855, 2007. doi: http://doi.org/10.1007/s11661-007-9226-2.

[16] SLÁMOVA, M., OCENÁSEK, V., VANDER VOORT, G., "Polarized light microscopy: Utilization in the investigation of the recrystallization of aluminum alloys", *Materials Characterization*, v. 53, n. 3, pp. 165–177, 2004. doi: http://doi.org/10.1016/j.matchar.2003.10.010.

[17] PADILHA, A.F., PLAUT, R.L., "Work hardening, recovery, recrystallization, and grain growth", In: Totten, G.E, Scott-MacKenzie, D. (eds), *Handbook of aluminum. Volume 2: alloy production and materials manufacturing*, 1 ed., chapter 6, New York, USA, Marcel Dekker, 2003. doi: http://doi.org/10.1201/9780429223259-6.

[18] SOUZA, S.H., PLAUT, R.L., LIMA, N.B., *et al*., "The occurrence of a peripheral coarse grain zone (PCGZ) in extruded bars of AA 7108", *Materials Science Forum*, v. 1016, pp. 1141–1146, 2021. doi: http://doi.org/10.4028/www.scientific.net/MSF.1016.1141.

[19] MARTINS, J.D., PADILHA, A.F., "Caracterização da liga comercial de alumínio 3003 produzida por fundição contínua de chapas ("twin roll caster"): textura cristalográfica", *REM. Revista Escola de Minas*, v. 60, n. 3, pp. 565–569, 2007. doi: http://doi.org/10.1590/S0370-44672007000300019.

[20] RAABE, D.., "Texture-property relationships in aluminum alloys: simulations and experiments", In: Totten, G.E., Scott-MacKenzie, D. (eds), *Handbook of aluminum. Volume 2: Alloy production and materials manufacturing*, 1 ed., chapter 8, New York, USA, Marcel Dekker, 2003. doi: http://doi.org/10.1201/9780203912607.ch8.

[21] GOW, K.V., "Secondary recrystallization in aluminium extrusions", *Acta Metallurgica*, v. 2, n. 3, pp. 394–405, 1954. doi: http://doi.org/10.1016/0001-6160(54)90057-7.

[22] ENGLER, O., "Control of texture and earing in aluminium alloy AA 3105 sheet for packaging applications", *Materials Science and Engineering A*, v. 538, pp. 69–80, 2012. doi: http://doi.org/10.1016/j.msea.2012.01.015.

[23] ENGLER, O., "Control of texture and earing in Al packaging sheet: a review", *Materials Science and Engineering A*, v. 56, pp. 2293–2306, 2025.

[24] MARTINS, A.L., COUTO, A.A., LIMA, N.B., *et al*., "Crystallographic texture evolution of aluminum alloy 3104 in the drawn and wall ironing (DWI) process", *Materials Research*, v. 22, pp. 1–6, 2019. doi: http://doi.org/10.1590/1980-5373-mr-2019-0037.

[25] MUZYK, M., PAKIELA, Z., KURZYDLOWSKI, K.J., "Generalized stacking fault energies of aluminum alloys: density functional theory calculations", *Metals*, v. 8, n. 10, pp. 823, 2018. doi: http://doi.org/10.3390/met8100823.

[26] MUZYK, M., PAKIELA, Z., KURZYDLOWSKI, K.J., "Ab initio calculations of the generalized stacking fault energy in aluminium alloys", *Scripta Materialia*, v. 64, n. 9, pp. 916–918, 2011. doi: http://doi.org/10.1016/j.scriptamat.2011.01.034.

[27] HUMPHREYS, F.J., HATHERLY, M., *Recrystallization and related annealing phenomena*, 2 ed., Amsterdam, Elsevier, 2004.

[28] WATERLOO, G., HANSEN, V., GJONNES, J., *et al*., "Effect of predeformation and preaging at room temperature in Al – Zn – Mg – (Cu, Zr) alloys", *Materials Science and Engineering A*, v. 303, n. 1–2, pp. 226–233, 2001. doi: http://doi.org/10.1016/S0921-5093(00)01883-9.

[29] MERRIMAN, C.C., FIELD, D.P., TRIVEDI, P., "Orientation dependence of dislocation structure evolution during cold rolling of aluminum", *Materials Science and Engineering A*, v. 494, n. 1–2, pp. 28–35, 2008. doi: http://doi.org/10.1016/j.msea.2007.10.090.

[30] PADILHA, A.F., SICILIANO JUNIOR, F., *Encruamento, recristalização, crescimento de grão e textura*, 3 ed., São Paulo, Edgard Blucher, 2005.